

Nonlinear Control of Quadrotor for Point Tracking: Actual Implementation and Experimental Tests

Young-Cheol Choi, *Student Member, IEEE*, and Hyo-Sung Ahn, *Member, IEEE*

Abstract—In this paper, a nonlinear control scheme along with its simulation and experimental results for a quadrotor are presented. It is not easy to control the quadrotor because the dynamics of quadrotor, which is obtained via the Euler–Lagrangian approach, has the features of underactuated, strongly coupled terms, uncertainty, and multiinput/multioutput. We propose a new nonlinear controller by using a backstepping-like feedback linearization method to control and stabilize the quadrotor. The designed controller is divided into three subcontrollers which are called attitude controller, altitude controller, and position controller. Stability of the designed controller is verified by the Lyapunov stability theorem. Detailed hardware parameters and experimental setups to implement the proposed nonlinear control algorithms are presented. The validity of proposed control scheme is demonstrated by simulations under different simulation scenarios. Experimental results show that the proposed controller is able to carry out the tasks of taking off, hovering, and positioning.

Index Terms—Autonomous flying test, backstepping, feedback linearization, quadrotor, tracking control.

I. INTRODUCTION

RECENTLY, autonomous aerial vehicles such as the quadrotor have attracted considerable amount of interest because of a wide area of applications and a lot of advantages. The quadrotor has many abilities such as the vertical take-off and landing, hover capability, high maneuverability, and agility. The quadrotor also possess more advantages than standard helicopters in terms of small size, efficiency, and safety. Due to these advantages, the quadrotor is eligible for applications like military services, surveillance, rescue, research area, remote inspection, and photography [1]–[5].

For autonomous flight of the quadrotor, one of the most important techniques is an efficient attitude control and stabilization. However, the control of the quadrotor is not easy because of the high nonlinearity, strongly coupled dynamics, and multi-variable nature. In addition, the quadrotor system is an underactuated system because the dynamics of a quadrotor have six outputs ($x, y, z, \phi, \theta, \psi$) while it has only four independent control inputs ($U_1 \sim U_4$). Uncertainties which are associated with physical parameters also bring another challenge for a control

Manuscript received March 3, 2014; revised May 28, 2014; accepted June 6, 2014. Date of publication June 5, 2014; date of current version May 18, 2015. Recommended by Technical Editor S. C. Mukhopadhyay. This work was supported by the National Research Foundation of Korea funded by the Korea government under Grant NRF-2013R1A2A2A01067449.

The authors are with the School of Mechatronics, Gwangju Institute of Science and Technology, Gwangju 500-712, Korea (e-mail: cyc@gist.ac.kr; hyosung@gist.ac.kr).

Color versions of one or more of the figures in this paper are available online at <http://ieeexplore.ieee.org>.

Digital Object Identifier 10.1109/TMECH.2014.2329945

design. Thus, it is hard to control the nonlinear and underactuated quadrotor system.

Different control strategies have been proposed to deal with the control problem of quadrotor. Linear control methods such as proportional-integral-derivative (PID) control and linear-quadratic regulator have been applied to solve this problem [2], [6]–[8]; however, the stability of these methods is only guaranteed in a restricted domain of flights. Nonlinear control methods can substantially expand the domain of controllable flights compared to linear controls.

Various nonlinear control methods such as linearization, saturation, backstepping, and sliding mode control were used to control the quadrotor system. For example, a nonlinear controller based on a decomposition into a nested structure and feedback linearization has been introduced [9]; a feedback linearization controller involving high-order derivative terms was proposed in [10]; and a feedback linearization was designed to control the attitude in an inner control loop [11]. However, in these linearization methods, only higher-level dynamics without consideration of physical parameters were considered. Backstepping control is another method that has been used to solve the nonlinear control problem of a quadrotor. An integral backstepping approach was applied into an autonomous flight of the quadrotor system including indoor experiments [3] and a backstepping control was used to stabilize the quadrotor's attitude system [4]. A new backstepping control strategy was applied to the quadrotor which can be seen as an interconnected subsystem [12]; a backstepping approach and parameter adaptive design were combined into the design of the adaptive controller for trajectory control problem [13]; and a new approach of the full state backstepping control scheme using sliding mode observer was proposed to the quadrotor [14]. However, in these backstepping approaches, aerodynamic effects and angular speed control in low-level motor system were not studied, which is the fundamental issue for a precise nonlinear control of a quadrotor. A sliding mode controller was proposed to stabilize the cascaded underactuated subsystem of quadrotor [15], and a control law was synthesized by sliding mode control based on the backstepping approach [16]. The sliding mode controller was tested to verify the flight mode of multipropeller multifunction aerial robot [17], and a dynamic inversion method with zero dynamics was used to control both linear and nonlinear systems, which involves an inner inversion loop [18]. Nested saturation control algorithm based on the Lyapunov analysis was proposed to track the desired trajectory including experimental tests [19]. However, in these sliding mode, dynamic inversion, and nested saturation approaches, the relationship among attitude, altitude, and position dynamics was not considered.

As outlined previously, although there have been some works to deal with the nonlinearity of quadrotor systems, in the most of these existing works, higher-level models for ideal environments have been considered. Moreover, the verification of the proposed control algorithms in the existing literature has been limited to simulation results. Even though a few papers introduced experimental tests [3], [4], [19]–[23], the tests were also limited to indoor cases in some ideal circumstances. However, for accurate outdoor tests and verifications, the physical parameters of the quadrotor dynamics should be considered precisely because the parameters affect the performance of quadrotor system significantly. As far as authors are concerned, there is no result on outdoor experiment for nonlinear tracking control taking account of overall system parameter problems.

In this paper, the detailed dynamics of the quadrotor, which is obtained by the Lagrange–Euler method, are presented for an outdoor nonlinear control of a quadrotor. We propose a new approach using backstepping-like feedback linearization which guarantees the stability in flights. The designed controller is divided into three subcontrollers: attitude controller, altitude controller, and position controller. To control the x, y position of quadrotor, the desired roll and pitch angles are considered. Mainly, we consider possible combinations of outputs (x, y, z, ψ) and virtual controller in order to track the given trajectory; during the tracking, two angles ϕ and θ are kept to be stable by attitude controller. The stability of designed control law is proved by the Lyapunov stability theorem. We implement the designed control algorithm into the quadrotor platform and verify the control law by experiments. Accordingly, we focus on the accurate simulation by using real physical parameters of quadrotor for ease of implementation and test on an actual quadrotor platform. For accurate simulations and experiments, we identify all physical parameters which are relevant with the quadrotor dynamics such as the moment of inertia, relation between the Brushless DC (BLDC) motor input and output, and aerodynamics effects empirically.

Consequently, the main contributions of this paper can be summarized as follows. First, this paper proposes a new nonlinear control algorithm and stability analysis based on the Lyapunov stability theorem considering detailed quadrotor dynamics. Second, for the actual implementation, this paper considers system parameters such as the moment of inertia, the relation between motor and battery, and aerodynamics effects. Third, the designed nonlinear controller is implemented into quadrotor system for outdoor experiments. Note that the existing nonlinear control algorithms have been mostly used in indoor tests under ideal environments. From comparative experimental tests, we see that our control algorithm shows a better performance than other existing nonlinear control algorithms.

II. QUADROTOR DYNAMIC MODEL AND PLATFORM

Before proceeding to explain the designed control law, the dynamics of flight motion is provided to understand the feature of quadrotor. Overall mechanisms of quadrotor maneuvers are shown in Fig. 1. The basic maneuvers are achieved by varying the current supplied to four different motors which

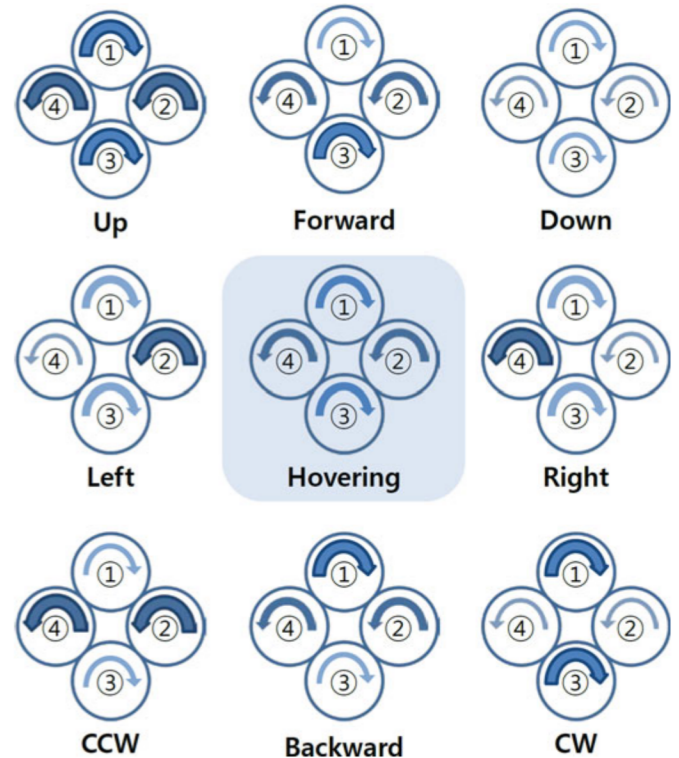


Fig. 1. Mechanism of quadrotor maneuvers.

change the force and torque balances acting on the quadrotor. An accurate mathematical dynamic model of quadrotor, which includes model uncertainties, is essential for designing a nonlinear controller. In the following section, we will describe the dynamic model of quadrotor and introduce experimental platform of quadrotor.

A. Dynamic Modeling

The dynamic model of quadrotor is derived using the *Euler-Lagrangian* approach. The full dynamics of attitude and position of the quadrotor is basically those of a rotating rigid body with six degrees of freedom. The structure of quadrotor including the free body diagram and coordinates system is shown in Fig. 2. Let $\mathbf{q} = (x, y, z, \phi, \theta, \psi) \in \mathbb{R}^6$ be the generalized coordinates where $\xi = (x, y, z) \in \mathbb{R}^3$ denotes the absolute position of the mass of the quadrotor relative to a fixed inertial frame. Euler angles, which are the orientation of the quadrotor, are expressed by $\eta = (\phi, \theta, \psi) \in \mathbb{R}^3$, where ϕ is the roll angle around the x axis, θ is the pitch angle around the y axis, and ψ is the yaw angle around the z axis. It is assumed that the Euler angles are bounded as follows:

$$\begin{aligned} \text{roll : } & -\frac{\pi}{2} \leq \phi \leq \frac{\pi}{2} \\ \text{pitch : } & -\frac{\pi}{2} \leq \theta \leq \frac{\pi}{2} \\ \text{yaw : } & -\pi \leq \psi < \pi. \end{aligned} \quad (1)$$

The dynamic model of quadrotor partitions into translational and rotational coordinates. The translational kinetic energy of

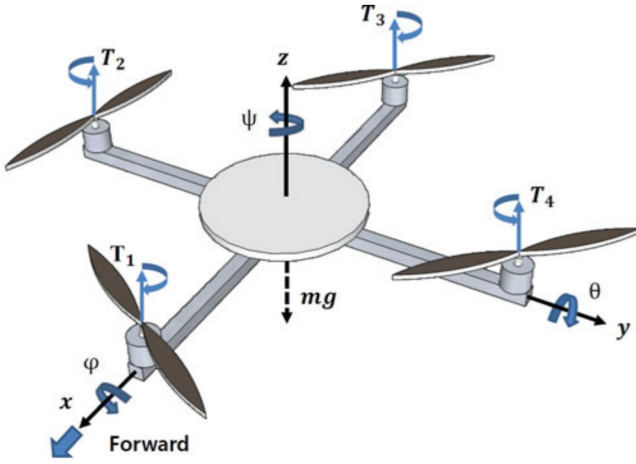


Fig. 2. Quadrotor configuration with a free body diagram.

the quadrotor is $T_{\text{trans}} = \frac{1}{2}m\dot{\xi}^T\dot{\xi}$ where m is the mass of quadrotor. The rotational kinetic energy is $T_{\text{rot}} = \frac{1}{2}I\dot{\eta}^T\dot{\eta}$. The matrix I is the moment of inertia matrix for the full-rotational kinetic energy of the quadrotor which is expressed directly in terms of the generalized coordinates η . The potential energy is $U = mgz$, which needs to be considered is the standard gravitational potential, where g is the acceleration due to gravity. Then, we can define the *Lagrangian* model as follows:

$$\begin{aligned} L(q, \dot{q}) &= T_{\text{trans}} + T_{\text{rot}} - U \\ &= \frac{1}{2}m\dot{\xi}^T\dot{\xi} + \frac{1}{2}I\dot{\eta}^T\dot{\eta} - mgz. \end{aligned} \quad (2)$$

The full quadrotor dynamics are obtained from the *Euler-Lagrangian* equations with external generalized force $F = (F_\xi, \tau)$ as follows:

$$\frac{d}{dt}\frac{\partial L}{\partial \dot{q}} - \frac{\partial L}{\partial q} = (F_\xi, \tau) \quad (3)$$

where F_ξ is the translational force applied to the quadrotor due to the throttle control input in the body frame, τ is the roll, pitch, and yaw moments. The translational force is $F_\xi = RF_R$ where R is the rotation matrix and F_R is the translational force in the inertial frame. The rotation matrix R equals to $R = R_zR_yR_x$, which is the orientation of the quadrotor. F_R is defined by

$$F_R = \begin{bmatrix} 0 \\ 0 \\ U_1 \end{bmatrix} \quad (4)$$

where U_1 is the main thrust. The main thrust is the summation of thrust moments as follows:

$$U_1 = T_1 + T_2 + T_3 + T_4 \quad (5)$$

where T_i is the thrust moment. The thrust moment is generated by each BLDC motor which is defined by

$$T_i = b\omega_i^2 \quad (6)$$

where b is a positive constant that denotes the thrust factor of propeller and ω_i is the angular velocity of the BLDC motor i .

Then, the generalized moments for the η variables are

$$\tau = \begin{bmatrix} \tau_\phi \\ \tau_\theta \\ \tau_\psi \end{bmatrix} = \begin{bmatrix} bl(\omega_4^2 - \omega_2^2) \\ bl(\omega_3^2 - \omega_1^2) \\ d(\omega_1^2 + \omega_3^2 - \omega_2^2 - \omega_4^2) \end{bmatrix} \quad (7)$$

where l is the distance from the motor to the center of gravity and d is the drag factor. Propeller coefficients b and d will be explained later. Thus, the control distribution from the four BLDC motors of the quadrotor is given by

$$\begin{bmatrix} U_1 \\ \tau_\phi \\ \tau_\theta \\ \tau_\psi \end{bmatrix} = \begin{bmatrix} b & b & b & b \\ 0 & -bl & 0 & bl \\ -bl & 0 & bl & 0 \\ d & -d & d & -d \end{bmatrix} \begin{bmatrix} \omega_1^2 \\ \omega_2^2 \\ \omega_3^2 \\ \omega_4^2 \end{bmatrix}. \quad (8)$$

If the required thrust and torque are given, we may solve for the rotor force using (8). We can combine $\dot{\xi}$ and $\dot{\eta}$ in (2) because the *Lagrangian* contains no cross terms in the kinetic energy. The *Euler-Lagrangian* equation can be partitioned into the dynamics for the ξ coordinates and η coordinates. Thus, the final model of the quadrotor is represented by

$$m\ddot{\xi} = - \begin{bmatrix} 0 \\ 0 \\ mg \end{bmatrix} + F_\xi \quad (9)$$

$$I\ddot{\eta} + \frac{d}{dt}\{I\}\dot{\eta} - \frac{1}{2}\frac{\partial}{\partial t}(\dot{\eta}^T I \dot{\eta}) = \tau. \quad (10)$$

The Coriolis–centripetal vector is defined by

$$\bar{V}(\eta, \dot{\eta}) = \dot{I}\dot{\eta} - \frac{1}{2}\frac{\partial}{\partial t}(\dot{\eta}^T I \dot{\eta}). \quad (11)$$

Then, we may write

$$I\ddot{\eta} + \bar{V}(\eta, \dot{\eta}) = \tau. \quad (12)$$

Here, $\bar{V}(\eta, \dot{\eta})$ can be expressed as

$$\begin{aligned} \bar{V}(\eta, \dot{\eta}) &= \left(I - \frac{1}{2}\frac{\partial}{\partial t}(\dot{\eta}^T I) \right) \dot{\eta} \\ &= C(\eta, \dot{\eta})\dot{\eta} \end{aligned} \quad (13)$$

where $C(\eta, \dot{\eta})$ is referred to as the *Coriolis* terms and contains the gyroscopic and centrifugal terms associated with the η dependence of I . This yields

$$\begin{aligned} m\ddot{\xi} &= F_\xi - mge_3 \\ I\ddot{\eta} &= \tau - C(\eta, \dot{\eta})\dot{\eta}. \end{aligned} \quad (14)$$

Finally, we can derive the dynamic model of the quadrotor in terms of translation (x, y, z) and rotation (ϕ, θ, ψ) as follows:

$$\begin{bmatrix} \ddot{x} \\ \ddot{y} \\ \ddot{z} \end{bmatrix} = \begin{bmatrix} c_\phi s_\theta c_\psi + s_\phi s_\psi \\ c_\phi s_\theta s_\psi - s_\phi c_\psi \\ c_\phi c_\theta \end{bmatrix} \frac{U_1}{m} + \begin{bmatrix} 0 \\ 0 \\ -g \end{bmatrix} \quad (15)$$

$$\begin{bmatrix} \ddot{\phi} \\ \ddot{\theta} \\ \ddot{\psi} \end{bmatrix} = f(\phi, \theta, \psi) + g(\phi, \theta, \psi)\tau_U \quad (16)$$

where c_ϕ is $\cos \phi$, s_ϕ is $\sin \phi$, and

$$f(\phi, \theta, \psi) = \begin{bmatrix} \dot{\theta}\dot{\psi}\left(\frac{I_y - I_z}{I_x}\right) - \frac{J_r}{I_x}\dot{\theta}\Omega \\ \dot{\phi}\dot{\psi}\left(\frac{I_z - I_x}{I_y}\right) + \frac{J_r}{I_y}\dot{\phi}\Omega \\ \dot{\phi}\dot{\theta}\left(\frac{I_x - I_y}{I_z}\right) \end{bmatrix}$$

$$g(\phi, \theta, \psi) = \begin{bmatrix} \frac{l}{I_x} & 0 & 0 \\ 0 & \frac{l}{I_y} & 0 \\ 0 & 0 & \frac{1}{I_z} \end{bmatrix}$$

and control inputs U_1, U_2, U_3 , and U_4 are governed by

$$U_1 = b(\omega_1^2 + \omega_2^2 + \omega_3^2 + \omega_4^2)$$

$$\tau_U = \begin{bmatrix} U_2 \\ U_3 \\ U_4 \end{bmatrix} = \begin{bmatrix} b(\omega_4^2 - \omega_2^2) \\ b(\omega_3^2 - \omega_1^2) \\ d(\omega_1^2 + \omega_3^2 - \omega_2^2 - \omega_4^2) \end{bmatrix} \in \mathbb{R}^3$$

where U_1 is essentially used to make the altitude reach the desired value, U_2 is used to control the roll and horizontal displacement, U_3 is used to control the pitch and vertical movement, U_4 is used to set the yaw displacement, $I_{x,y,z}$ are the moment of inertia of quadrotor, J_r is the moment of inertia of rotor, and $\sigma = \omega_1 - \omega_2 + \omega_3 - \omega_4$. Thus, the quadrotor system is the form of an underactuated system with six outputs and four control inputs.

B. Platform Preliminaries

For implementing the designed nonlinear controller and expanding hardware components, the flexibility of quadrotor in both hardware and software is important. In our research, we selected the Arducopter as main platform which is a quadrotor autopilot designed from the Arduino framework. The quadrotor platform was developed by integrating different mechanical and electrical components. The complete quadrotor system is illustrated in Fig. 3 which is composed of the structural frame, propulsion system, microcontroller unit for flying, external sensors, and power system. Details of each component are elaborated in the following sections.

1) *Structural Frame*: The quadrotor structure consists of the main center plate and four arms to support the propulsion system. The main plate is made of carbon fiber, which is lighter than aluminum plate for the same strength. Almost all components are installed on this main plate except for the propulsion system. Four arms are made of aluminum and they are connected to the main plate. Each arm has a skid system for landing and preventing damage of the quadrotor system, which is also made of carbon fiber.

2) *Propulsion System*: The propulsion system is composed of the BLDC motor, electronic speed controller, and propeller. Each component has its own performance characteristics and region of maximum efficiency. The selection and combination of each component is crucial in achieving an overall propulsion

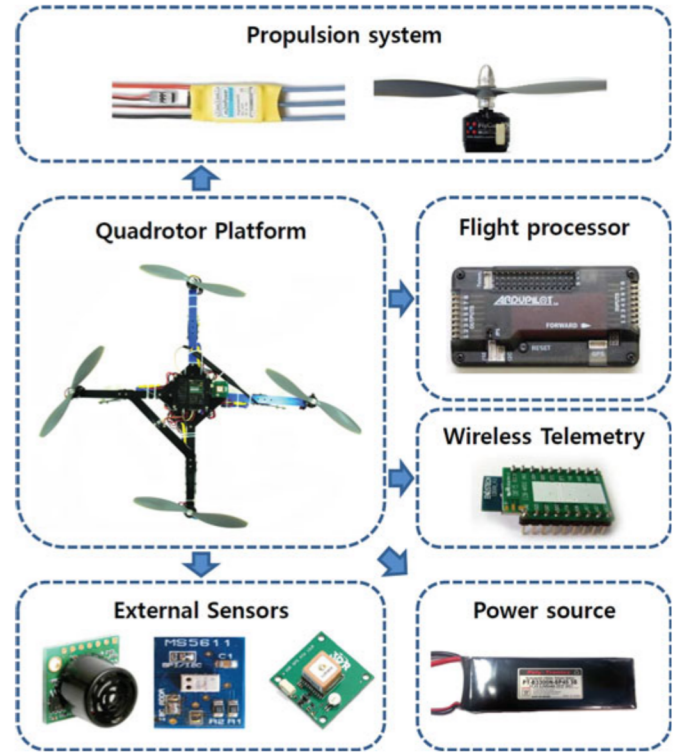


Fig. 3. Configuration of the quadrotor.

system which is well suited to the application and efficient [24], [25]. The Flycam 925 kV BLDC motor is selected considering the efficiency and performance of the quadrotor. The weight of this motor is 0.53 N and the maximum thrust is 7.845 N. The Arducopter 20 Amp electronic speed controller is chosen to operate the BLDC motor. This electronic speed controller has low output resistance and can be programmed. A slow flyer propeller with size of 10×4.7 is used for generating thrust moments. Each set contains a pusher (clockwise rotation) and a puller (counter clockwise rotation) propeller.

3) *Flight Microcontroller Processor and Attitude and Heading Reference System*: For onboard processing and operations of the implemented control law, the Arduino Atmega 2560 embedded processor is used. The Arduino, which has well organized device driver library for various sensors and actuators, is the name of both the open-source single board microcontroller unit and the integrated development environment. The Arduino is easy to install, and firmware can be easily downloaded using a serial port. Furthermore, there are a lot of libraries related to hardware peripherals and signal analysis. The inertial measurement unit, which consists of three-axis accelerometer and gyroscope, is integrated on the main board. A digital compass (HMC5883), which called magnetometer, is connected to the inertial measurement unit through an I2C port and that completes the attitude and heading reference system for the quadrotor platform.

4) *External Sensors and Wireless Telemetry*: An ultrasonic sensor (MB1000 LV-MaxSonar-EZ0) is installed in the main plate for measuring the altitude of quadrotor. We can use the

ultrasonic sensor only in row altitude, because the detecting range of the ultrasonic sensor is limited to 6.5 m. The barometric pressure sensor (MS5611) is used to complement the ultrasonic sensor. The global positioning system (GPS) module (MT3329) is used for a navigation purpose and it is connected through a serial connection to the flight processor. Zigbee module (EZBee-M100) is installed to obtain flight data for autonomous flying test. The Zigbee is a popular wireless communication system due to its simple setup, low cost, and reasonable communication range.

5) *Power Supply System*: The power source is important in maintaining good performance and long flight time. The power system should have huge capacities, high energy density, and low weight. The lithium polymer battery, which shows better performances compared to other types of batteries, is used to satisfy these requirements. Thus, the lithium polymer battery that is considered ideal is a three-cell pack with 11.1 V, 3300 mAh capacity, and 45 C maximum for the continuous current output.

III. PHYSICAL PARAMETER PROBLEMS

As mentioned previously, the mathematical modeling of the quadrotor is crucial for control; however, the dynamics of the quadrotor always include some uncertainties in the mass, the moment of inertia, and aerodynamics effects. In this section, we will discuss physical parameters which are concerned with uncertainty factors of quadrotor dynamics.

A. Moment of Inertia

The moment of inertia is an important parameter for the accurate dynamic modeling of system. Thus, measurements or computational estimations of moment of inertia are needed during the design and identification of quadrotor dynamics. It can be computed analytically by summing the contributions of all the individual elements of quadrotor; however, this method is not easy to apply into composite assembled system. In this paper, we consider experimental technique for measuring the moment of inertia of quadrotor. The bifilar (two-wire) torsional method is an apparatus that has been used for measuring the moment of inertia of aerial vehicles because of its simplicity, safety, and relatively high accuracy [26]. The bifilar torsional method, as shown in Fig. 4, consists of a test object suspended by two thin wires, which have same length, of height h and separation displacements a and b from the quadrotor center of gravity. The quadrotor is rendered to oscillate around a vertical axis through its center by human operator. The period of oscillation is recorded. The bifilar torsional method is easily defined by its kinetic and potential energy via *Lagrangian* dynamics formulation. The total kinetic energy can be changed into the rotational kinetic energy of the quadrotor by omitting the small amount of kinetic energy in the suspension wires. The gravitational potential energy can be obtained by omitting the energy of the support wires, which is small enough to ignore. From the nonlinear *Lagrangian* equation, we can obtain the simplified *Lagrangian* equation by assuming that the angular motion is small, and by omitting damping. Using the simplified

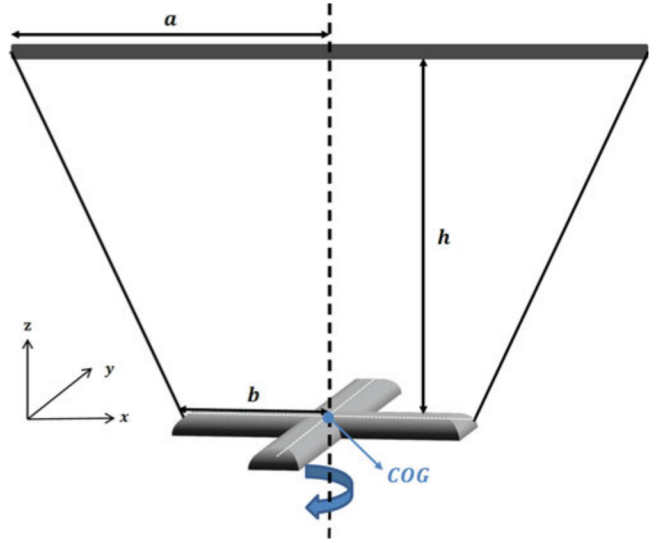


Fig. 4. Bifilar torsional method.

TABLE I
PARAMETERS OF THE BIFILAR TORSIONAL METHOD

Test #	m (kg)	g (m/s ²)	a (m)	b (m)	h (m)
Test 1	1.336	9.80665	0.535	0.285	0.605
Test 2	1.336	9.80665	0.6175	0.285	0.595
Test 3	1.336	9.80665	0.4675	0.285	0.656

Lagrangian equation, the movement of the quadrotor can be represented as follows:

$$\ddot{\theta} + \frac{abW}{I_z h} \theta = 0 \quad (17)$$

where a and b are displacement from center of gravity, h is the height, and W is the weight of quadrotor. Thus, the oscillation frequency can be described by

$$\omega^2 = \left(\frac{2\pi}{T} \right)^2 = \frac{abW}{I_z h}. \quad (18)$$

From (18), we can calculate the moment of inertia I_z as follows:

$$I_z = \left(\frac{T}{2\pi} \right)^2 \frac{abW}{h}. \quad (19)$$

In experiments, ten set of data are measured for ten oscillations with angular displacement of the system with different parameters a , b , and h . We carried out three tests with different parameters and the used parameters of the bifilar torsional method are given in Table I.

The results of the experiment for measuring oscillation time are presented in Table II. The period of the average oscillation is measured as 0.698 s. Using this value, we can calculate the moment of inertia about a vertical axis z using (19). The moment of inertia of other axes also can be calculated by the same way.

TABLE II
MEASURED OSCILLATION TIME (z -AXIS)

Run #	Test 1	Test 2	Test 3
	Time (s) (10 oscillations)		
1	6.9	6.4	7.7
2	6.8	6.3	7.7
3	6.9	6.3	7.7
4	6.9	6.4	7.6
5	6.9	6.4	7.7
6	6.8	6.4	7.7
7	6.9	6.3	7.7
8	7.0	6.3	7.8
9	6.9	6.4	7.7
10	6.9	6.4	7.6
Average	0.688	0.636	0.769

TABLE III
MOMENT OF INERTIA OF THE QUADROTOR

	Value	Unit
I_x	0.0259	$\text{kg} \cdot \text{m}^2$
I_y	0.0260	
I_z	0.0397	

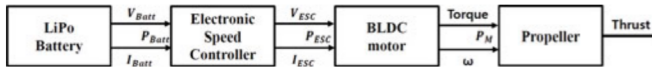


Fig. 5. Electric propulsion system of the quadrotor.

Consequently, we can obtain the moment of inertia of quadrotor through experiments and results are presented in Table III.

B. Electric Propulsion System

The electric propulsion system of quadrotor is composed of the BLDC motor, electronic speed controller, and propeller. Fig. 5 illustrates the electric propulsion system and power transfer through four components of the propulsion system. The power derived from the lithium polymer battery is given by

$$P_{\text{batt}} = V_{\text{batt}} \times I_{\text{batt}} \quad (20)$$

where V_{batt} is the battery voltage and I_{batt} is the current. The electric propulsion system converts electrical power to mechanical power in the form of thrust. Each BLDC motor has the electronic speed controller that receives command from the main controller unit in pulse-width-modulation (PWM) form. The BLDC motor converts the electrical power into a torque on its output shaft at an angular velocity ω given by

$$P_M = \text{Torque} \times \omega. \quad (21)$$

The power is derived from the battery source that is reduced during the flight time with a nonlinear slope. Decreasing in voltage of the battery is severely modulated due to the electrical interactions in propulsion system. The battery condition is relevant to the angular speed of the BLDC motor, and the angular speed is relevant to the thrust of quadrotor. Thus, according to the battery condition, the output thrust will not be constant

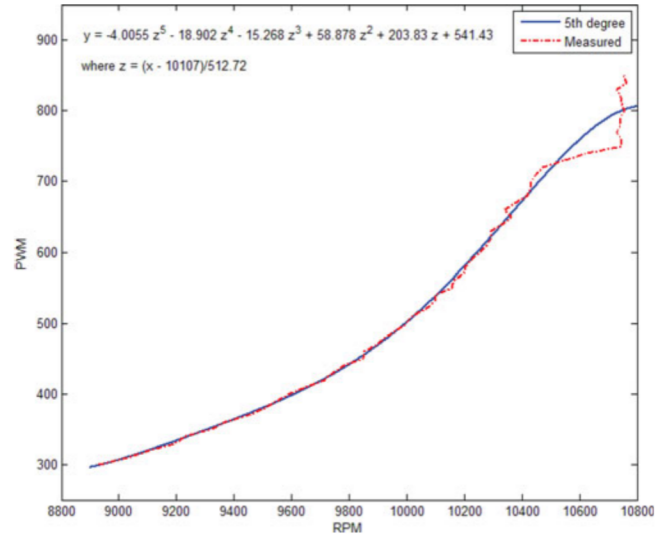


Fig. 6. Relation between input PWM and output RPM.

while the control input PWM value is not changed. Furthermore, the propeller imposes a nonlinear load on the BLDC motor because of aerodynamic effects. Therefore, it is important to know the relationship between the control input PWM and the output angular velocity ω in different battery conditions for the stable flying. We measured the angular velocity of the BLDC motor in various battery conditions. To measure the relationship between the PWM and angular velocity, the photo sensor is used. On the outer side of BLDC motor, two different color covers are attached and the photo sensor is installed perpendicular to the BLDC motor while keeping a suitable distance. By measuring interval time of signal, which is obtained by two different color covers, the rotation speed of the BLDC motor can be obtained. In order to find the relation between the control input PWM and the angular velocity, the rotation speed is measured at every ten PWM step. To obtain accuracy data, we measured the relationship 30 times in different battery conditions and the mean value is used in actual implementation. The relation between input and output data and fitting curve are depicted in Fig. 6. Range of output [i.e., revolutions-per-minute (RPM)], is limited to from 8800 to 10 800 RPM because of the motor and flight conditions. We have used 925-kV BLDC motor and 11.1-V battery; thus, the maximum RPM, which is around 10 800 RPM, can be calculated by multiplying the RPM constant (925 kV) and the average voltage (11.7 V). Using a fifth order polynomial fitting curve, which is offered by MATLAB, the relationship between the input PWM and output RPM can be obtained as follows:

$$f(n) = p_5 n^5 + p_4 n^4 + p_3 n^3 + p_2 n^2 + p_1 n + p_0 \quad (22)$$

where $n = \frac{(\text{RPM} - 10107)}{512.72}$ and $p_0 \sim p_5$ are coefficient values as follows:

$$p_0 = -4.0055, p_1 = -18.902, p_2 = -15.268$$

$$p_3 = 58.878, p_4 = 203.83, p_5 = 541.43.$$

TABLE IV
PROPELLER PARAMETERS

Name	Parameter	Value	Units
Radius	r	0.127	m
Thrust coeff.	C_T	0.1225	-
Power coeff.	C_P	0.0510	-
Air density (15 °C)	ρ	1.225	kg/m ³
Span area	A	0.0507	m ²

Consequently, the control input PWM is calculated by (22) when the desired angular velocity of each BLDC motor is given by the controller.

C. Aerodynamics Effects of Propeller

The aerodynamics of propeller has been extensively studied during several decades with the development of manned aerial vehicle [27]–[29]. These aerodynamics models are useful for the design of rotor systems, where all parameters of propeller are fundamental to the design problem. Although aerodynamics effects of the quadrotor vehicle are often assumed to be accurately modeled as linear for a control, this assumption is only reasonable when the rotation speed of propeller is low. Thus, the impact of the aerodynamics effects resulting from variations of rotation needs to be considered. In this paper, we would like to address a basic level of aerodynamic problem of propeller. The thrust moment, which is denoted by (6), generated by a hovering rotor in free air may be modeled using momentum theory [28]. The thrust factor b is defined by

$$b = C_T \rho A r^2 \quad (23)$$

where C_T is the thrust coefficient, ρ is the air density, A is the propeller span area, and r is the radius of the propeller. The thrust coefficient C_T depends on the propeller geometry and aerodynamics characteristics that is derived using a combination of momentum and blade theory [29]. Thus, the thrust moment can be rewritten as follows:

$$T_i = b\omega_i^2 = C_T \rho A r^2 \omega_i^2. \quad (24)$$

The thrust moment causes a drag moment on the rotor that acts opposite to the direction. The drag factor d is defined by

$$d = C_P \rho A r^3 \omega_i^2 \quad (25)$$

where C_P is the power coefficient of propeller. The thrust and power coefficient can be determined by static thrust tests which are given by manufacturer's or propeller database site [30].

The propeller determines the relationship between motor speed and load torque. In this paper, we selected 10×4.7 propeller whose size is a 10-inch diameter with a pitch of 4.7 inch per revolution. Based on the manufacturer's database, geometry data and aerodynamics parameters are shown in Table IV. From (23), (25), and Table IV, we can obtain the thrust factor $b = 1.22641e^{-4}$ and drag factor $d = 6.48447e^{-6}$.

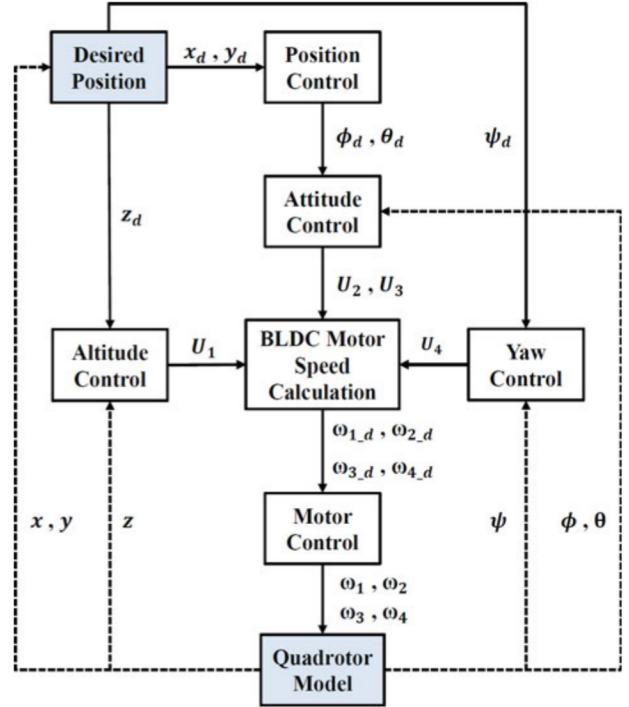


Fig. 7. Control schematic of the quadrotor.

IV. NONLINEAR CONTROLLER DESIGN AND STABILITY ANALYSIS

In this section, we consider a nonlinear controller of the quadrotor which includes attitude control for stabilization, altitude control, and position control for tracking problem. The main objective of designed controller is to ensure that the position of quadrotor (x, y, z, ψ) tracks the desired trajectory (x_d, y_d, z_d, ψ_d) asymptotically. The attitude controller is to design control inputs $U_2 \sim U_4$ such that the Euler angles [ϕ, θ, ψ] follow the desired attitude trajectory [ϕ_d, θ_d, ψ_d] which are derived from the position controller. Overall control schematic is shown in Fig. 7 and stability analysis of the designed controller is verified by Lyapunov stability theorem.

A. Attitude Controller

Attitude control of the quadrotor is the crucial part for stabilization and tracking control problem. We first define errors associated with the attitude dynamics of the quadrotor as follows:

$$e_1 = \phi - \phi_d \quad (26)$$

$$e_2 = \dot{\phi} - \dot{\phi}_d + k_1 e_1 \quad (27)$$

$$e_3 = \theta - \theta_d \quad (28)$$

$$e_4 = \dot{\theta} - \dot{\theta}_d + k_3 e_3 \quad (29)$$

$$e_5 = \psi - \psi_d \quad (30)$$

$$e_6 = \dot{\psi} - \dot{\psi}_d + k_5 e_5. \quad (31)$$

Obviously, the error e_2 converges to zero when e_1 is zero. Using these Euler angle errors, we can define the Lyapunov function to check the stability of attitude controller. Let us consider the Lyapunov candidate V_1 as follows:

$$V_1 = \frac{1}{2} \{ e_1^2 + e_2^2 + e_3^2 + e_4^2 + e_5^2 + e_6^2 \} \quad (32)$$

where the Lyapunov candidate V_1 is positive definite and the time derivative of the Lyapunov candidate V_1 is defined by

$$\dot{V}_1 = e_1 \dot{e}_1 + e_2 \dot{e}_2 + e_3 \dot{e}_3 + e_4 \dot{e}_4 + e_5 \dot{e}_5 + e_6 \dot{e}_6. \quad (33)$$

Thus, the time derivative of Lyapunov function V_1 in (33) can be rewritten as follows:

$$\begin{aligned} \dot{V}_1 &= e_1 \dot{e}_1 + e_2 \dot{e}_2 + e_3 \dot{e}_3 + e_4 \dot{e}_4 + e_5 \dot{e}_5 + e_6 \dot{e}_6 \\ &= e_1(e_2 - k_1 e_1) + e_2(\ddot{\phi} - \ddot{\phi}_d + k_1 \dot{e}_1) \\ &\quad + e_3(e_4 - k_3 e_3) + e_4(\ddot{\theta} - \ddot{\theta}_d + k_3 \dot{e}_3) \\ &\quad + e_5(e_6 - k_5 e_5) + e_6(\ddot{\psi} - \ddot{\psi}_d + k_5 \dot{e}_5). \end{aligned} \quad (34)$$

For the stabilization of quadrotor, the time derivatives of desired angular rates are assumed to be zero ($\ddot{\phi}_d = \ddot{\theta}_d = \ddot{\psi}_d = 0$); then, we can rewrite (34) as follows:

$$\begin{aligned} \dot{V}_1 &= e_1 \dot{e}_1 + e_2 \dot{e}_2 + e_3 \dot{e}_3 + e_4 \dot{e}_4 + e_5 \dot{e}_5 + e_6 \dot{e}_6 \\ &= e_1(e_2 - k_1 e_1) + e_3(e_4 - k_3 e_3) + e_5(e_6 - k_5 e_5) \\ &\quad + e_2 \left\{ \dot{\theta} \psi \left(\frac{I_y - I_z}{I_x} \right) - \frac{J_r}{I_x} \dot{\theta} \Omega \right. \\ &\quad \left. + \frac{l}{I_x} U_2 + k_1(e_2 - k_1 e_1) \right\} \\ &\quad + e_4 \left\{ \dot{\phi} \psi \left(\frac{I_z - I_x}{I_y} \right) + \frac{J_r}{I_y} \dot{\phi} \Omega \right. \\ &\quad \left. + \frac{l}{I_y} U_3 + k_3(e_4 - k_3 e_3) \right\} \\ &\quad + e_6 \left\{ \dot{\phi} \dot{\theta} \left(\frac{I_x - I_y}{I_z} \right) + \frac{1}{I_z} U_4 + k_5(e_6 - k_5 e_5) \right\}. \end{aligned} \quad (35)$$

The time derivative of Lyapunov candidate \dot{V}_1 should be seminegative definite, thus control inputs $U_2 \sim U_4$ for the attitude control can be obtained by using the following control laws:

$$\begin{aligned} U_2 &= \frac{I_x}{l} \left\{ -\dot{\theta} \psi \left(\frac{I_y - I_z}{I_x} \right) + \frac{J_r}{I_x} \dot{\theta} \Omega \right. \\ &\quad \left. + (k_1^2 - 1)e_1 - (k_1 + k_2)e_2 \right\} \\ U_3 &= \frac{I_y}{l} \left\{ -\dot{\phi} \psi \left(\frac{I_z - I_x}{I_y} \right) - \frac{J_r}{I_y} \dot{\phi} \Omega \right. \\ &\quad \left. + (k_3^2 - 1)e_3 - (k_3 + k_4)e_4 \right\} \\ U_4 &= I_z \left\{ -\dot{\phi} \dot{\theta} \left(\frac{I_x - I_y}{I_z} \right) + (k_5^2 - 1)e_5 - (k_5 + k_6)e_6 \right\} \end{aligned} \quad (36)$$

where $k_1 \sim k_6$ are control parameters which are positive constants. These control parameters should be carefully chosen to ensure a stable well-damped response. The time derivative of the designed Lyapunov function is as follows:

$$\dot{V}_1 = -k_1 e_1^2 - k_2 e_2^2 - k_3 e_3^2 - k_4 e_4^2 - k_5 e_5^2 - k_6 e_6^2 \leq 0. \quad (37)$$

Consequently, the attitude dynamics (16) is asymptotically stable by using the designed control inputs (36).

B. Altitude Controller

From (15), the altitude subsystem is controlled by using the vertical force control input U_1 which is the summation of the thrust moment of each motor. Thus, let us consider the altitude error e_7 and e_8 as follows:

$$e_7 = z - z_d \quad (38)$$

$$e_8 = \dot{z} - \dot{z}_d + k_7 e_7 \quad (39)$$

where k_7 is the control parameter which is positive constant and the error e_8 is converged to zero when error e_7 is zero. From these error definitions, we can define the Lyapunov candidate V_2 to stabilize the altitude control system as follows:

$$V_2 = \frac{1}{2} (e_7^2 + e_8^2). \quad (40)$$

Then, the time derivative of Lyapunov candidate can be denoted by

$$\begin{aligned} \dot{V}_2 &= e_7 \dot{e}_7 + e_8 \dot{e}_8 = e_7 \dot{e}_7 + e_8 (\ddot{z} - \ddot{z}_d + k_7 \dot{e}_7) \\ &= e_7 \dot{e}_7 + e_8 \left\{ (\cos \phi \cos \theta) \frac{1}{m} U_1 - g - \ddot{z}_d + k_7 \dot{e}_7 \right\} \\ &= e_7(e_8 - k_7 e_7) + e_8 \left\{ (\cos \phi \cos \theta) \frac{1}{m} U_1 - g - \ddot{z}_d \right. \\ &\quad \left. + k_7(e_8 - k_7 e_7) \right\}. \end{aligned} \quad (41)$$

We assumed that the time derivative of desired velocity of the altitude is zero ($\ddot{z}_d = 0$). According to the Lyapunov stability theorem, the time derivative (41) should be seminegative definite; thus the control input U_1 can be defined as follows:

$$U_1 = \frac{m \{ g + (k_7^2 - 1)e_7 - (k_7 + k_8)e_8 \}}{\cos \phi \cos \theta} \quad (42)$$

where k_8 is control parameter which is positive definite. When ϕ or θ equals to $\frac{\pi}{2}$ or $-\frac{\pi}{2}$, the control input U_1 cannot exist because the denominator of U_1 equals to zero. Thus, the boundary condition of the Euler angles in (1) is defined in the previous section. The time derivative of Lyapunov candidate is seminegative definite as follows:

$$\dot{V}_2 = -k_7 e_7^2 - k_8 e_8^2 \leq 0. \quad (43)$$

Therefore, the altitude control is asymptotically stable.

C. Position Controller

Attitude and altitude controllers of quadrotor are designed by using Lyapunov-based control method; however, overall control

system of quadrotor is an underactuated system with four control inputs and six outputs because dynamics of x , y positions are coupled with dynamics of the Euler angle. Thus, we consider the virtual controller to obtain the desired Euler angles for position control. Let us consider x , y errors in the *Cartesian* coordinate, which are received by the GPS module, as follows:

$$e_9 = x - x_d \quad (44)$$

$$e_{10} = \dot{x} - \dot{x}_d + k_9 e_9 \quad (45)$$

$$e_{11} = y - y_d \quad (46)$$

$$e_{12} = \dot{y} - \dot{y}_d + k_{11} e_{11} \quad (47)$$

where x_d and y_d are the desired position in global coordinate system, and control parameters k_9 and k_{11} are positive. In order to check the stability of the position controller, the Lyapunov candidate V_3 is defined by

$$V_3 = \frac{1}{2}(\zeta_1 e_9^2 + \zeta_2 e_{10}^2 + \zeta_3 e_{11}^2 + \zeta_4 e_{12}^2) \quad (48)$$

and the time derivative of Lyapunov candidate \dot{V}_3 can be obtained by

$$\begin{aligned} \dot{V}_3 &= \zeta_1 e_9 \dot{e}_9 + \zeta_2 e_{10} \dot{e}_{10} + \zeta_3 e_{11} \dot{e}_{11} + \zeta_4 e_{12} \dot{e}_{12} \\ &= \zeta_1 e_9 (e_{10} - k_9 e_9) + \zeta_3 e_{11} (e_{12} - k_{11} e_{11}) \\ &\quad + \zeta_2 e_{10} \{\ddot{x} - \ddot{x}_d + k_9 (e_{10} - k_9 e_9)\} \\ &\quad + \zeta_4 e_{12} \{\ddot{y} - \ddot{y}_d + k_{11} (e_{12} - k_{11} e_{11})\}. \end{aligned} \quad (49)$$

We can find \ddot{x} and \ddot{y} from the position dynamics of quadrotor in (15). Assume that the time derivative of desired position \dot{x}_d and \dot{y}_d are zero, which means \ddot{x}_d and \ddot{y}_d are also zero. Then, we can rewrite the time derivative of Lyapunov function as follows:

$$\begin{aligned} \dot{V}_3 &= \zeta_1 e_9 e_{10} - \zeta_1 k_9 e_9^2 + \zeta_3 e_{11} e_{12} - \zeta_3 k_{11} e_{11}^2 \\ &\quad + \zeta_2 e_{10} \gamma_1 \frac{U_1}{m} + \zeta_2 k_9 e_{10}^2 - \zeta_2 k_9^2 e_9 e_{10} \\ &\quad + \zeta_4 e_{12} \gamma_2 \frac{U_1}{m} + \zeta_4 k_{11} e_{12} - \zeta_4 k_{11}^2 e_{11} e_{12} \end{aligned} \quad (50)$$

where $\gamma_1 = \cos \phi \sin \theta \cos \psi + \sin \phi \sin \psi$ and $\gamma_2 = \cos \phi \sin \theta \sin \psi - \sin \phi \cos \psi$

The time derivative of Lyapunov candidate \dot{V}_3 should be less than or equal to zero to satisfy the Lyapunov stability theorem.

Theorem 1: Consider the time derivative of Lyapunov function \dot{V}_3 in (50). Then, asymptotically stability can be guaranteed, provided that k_9 and k_{11} are large enough,

Proof: We can rewrite the Lypunov stability condition in (50) by choosing $\zeta_1 = \zeta_2 k_9^2$ and $\zeta_3 = \zeta_4 k_{11}^2$ as:

$$\begin{aligned} \dot{V}_3 &= \zeta_2 e_{10} \gamma_1 \frac{U_1}{m} + \zeta_2 k_9 e_{10}^2 - \zeta_2 k_9^3 e_9^2 \\ &\quad + \zeta_4 e_{12} \gamma_2 \frac{U_1}{m} + \zeta_4 k_{11} e_{12}^2 - \zeta_4 k_{11}^3 e_{11}^2 \leq 0. \end{aligned} \quad (51)$$

If control parameters k_9 and k_{11} are large enough, then

$$k_9 e_{10}^2 - k_9^3 e_9^2 < 0 \Rightarrow k_9 > \left| \frac{e_{10}}{e_9} \right|$$

$$k_{11} e_{12}^2 - k_{11}^3 e_{11}^2 < 0 \Rightarrow k_{11} > \left| \frac{e_{12}}{e_{11}} \right|. \quad (52)$$

Thus, the following condition should be ensured to satisfy the stability.

$$\dot{V}_3 = \zeta_2 e_{10} \gamma_1 \frac{U_1}{m} + \zeta_4 e_{12} \gamma_2 \frac{U_1}{m} \leq 0 \quad (53)$$

where the mass m , control parameters ζ_2 , ζ_4 , and the altitude control input U_1 are always positive. Thus, by considering the sign of e_{10} and e_{12} , if we could choose γ_1 and γ_2 , in absolute magnitude, less than virtual inputs γ_1^{sol} and γ_2^{sol} ; but under the same sign as γ_1^{sol} and γ_2^{sol} , (i.e., $|\gamma_1| \leq |\gamma_1^{\text{sol}}|$ and $|\gamma_2| \leq |\gamma_2^{\text{sol}}|$) via proper choices of ϕ , θ , and ψ such as

$$\gamma_1^{\text{sol}} = \begin{cases} \gamma_1^{\max}, & \text{if } e_{10} \geq 0 \\ -\gamma_1^{\max}, & \text{if } e_{10} < 0 \end{cases} \quad (54)$$

$$\gamma_2^{\text{sol}} = \begin{cases} \gamma_2^{\max}, & \text{if } e_{12} \geq 0 \\ -\gamma_2^{\max}, & \text{if } e_{12} < 0 \end{cases} \quad (55)$$

where $\gamma_1^{\max} > 0$ and $\gamma_2^{\max} > 0$, then, $\dot{V}_3 \leq 0$ is ensured.

In the aforementioned theorem, γ_1 and γ_2 are functions of Euler angles. So, we cannot choose them arbitrary large; thus, γ_1^{\max} and γ_2^{\max} should be bounded according to the possible magnitude of γ_1 and γ_2 . The following result provides a guideline for this choice.

Lemma 1: Virtual control inputs γ_1^{sol} and γ_2^{sol} should be bounded as follows:

$$\begin{cases} \gamma_1^{\text{sol}} \leq |0.7071| \\ \gamma_2^{\text{sol}} \leq |0.7071| \end{cases} \quad (56)$$

Proof: According to the assumption of Euler angles, γ_1 and γ_2 are bounded as follows:

$$\begin{cases} -1 \leq \gamma_1 \leq 1 \\ -1 \leq \gamma_2 \leq 1 \end{cases} \quad (57)$$

Consider virtual controllers γ_1^{sol} and γ_2^{sol} to find the desired Euler angle ϕ_d and θ_d . By subtracting $\gamma_2 \times \frac{1}{\sin \psi}$ from $\gamma_1 \times \frac{1}{\cos \psi}$, we have

$$\begin{aligned} &\cos \phi \sin \theta + \sin \phi \frac{\sin \psi}{\cos \psi} - \cos \phi \sin \theta + \sin \phi \frac{\cos \psi}{\sin \psi} \\ &= \sin \phi \left(\frac{\sin \psi}{\cos \psi} + \frac{\cos \psi}{\sin \psi} \right) = \gamma_1^{\text{sol}} \frac{1}{\sin \psi} - \gamma_2^{\text{sol}} \frac{1}{\cos \psi}. \end{aligned} \quad (58)$$

Thus, from (58), we can calculate $\sin \phi$ as follows:

$$\sin \phi = \gamma_1^{\text{sol}} \sin \psi - \gamma_2^{\text{sol}} \cos \psi. \quad (59)$$

TABLE V
COMPARISONS OF SIMULATION RESULTS—POSITIONS

Benchmarks		Rise time	Max overshoot	Settling time
Designed	<i>x</i>	2.50 s	0 % (3.91e-08)	2.70 s
	<i>y</i>	2.50 s	0 % (-3.33e-13)	2.70 s
	<i>z</i>	2.68 s	0.53 %	2.87 s
Nonlinear1 [19]	<i>x</i>	2.62 s	22.07 %	7.92 s
	<i>y</i>	2.62 s	22.02 %	7.92 s
	<i>z</i>	13.51 s	16.45 %	35.29 s
Nonlinear2 [23]	<i>x</i>	1.61 s	5.45 %	3.11 s
	<i>y</i>	1.62 s	5.45 %	3.11 s
	<i>z</i>	3.47 s	7.46 %	7.37 s

From the boundary of ϕ , $\sin \phi$ is bounded between -1 to 1 . So, from the aforementioned equation, we have

$$\begin{aligned} & ((\gamma_1^{\text{sol}})^2 + (-\gamma_2^{\text{sol}})^2) (\sin^2 \psi + \cos^2 \psi) \\ & \geq (\gamma_1^{\text{sol}} \sin \psi + (-\gamma_2^{\text{sol}}) \cos \psi)^2 \end{aligned} \quad (60)$$

where $\sin^2 \psi + \cos^2 \psi = 1$ and $(\gamma_1^{\text{sol}} \sin \psi + (-\gamma_2^{\text{sol}}) \cos \psi)^2 = \sin^2 \phi$. Thus, we can rewrite (60) as follows:

$$(\gamma_1^{\text{sol}})^2 + (\gamma_2^{\text{sol}})^2 \geq \sin^2 \phi. \quad (61)$$

When $(\gamma_1^{\text{sol}})^2$ equals to $(\gamma_2^{\text{sol}})^2$, it has the maximum value 1 (i.e., $(\gamma_1^{\text{max}})^2 = 1$). Thus, we can obtain the boundary of γ_1^{sol} as follows:

$$2(\gamma_1^{\text{sol}})^2 \leq 1. \quad (62)$$

Hence, we have $\gamma_1^{\text{sol}} \leq |0.7071|$. Similarly, for γ_2^{sol} , we have $\gamma_2^{\text{sol}} \leq |0.7071|$. ■

Consequently, by choosing $\gamma_1^{\text{sol}} \leq |0.7071|$ and $\gamma_2^{\text{sol}} \leq |0.7071|$, we can obtain the desired roll and pitch angles to track the desired position.

V. SIMULATION RESULTS

Simulation results are provided in this section to illustrate the stability property and performance of the proposed controller. All physical parameters of the quadrotor, which are based on the real quadrotor platform, are used in simulation results. The following values have been chosen for the control parameters: $k_1 \sim k_4 = 2.5$, $k_5, k_6 = 2.0$, $k_7 = 2.2$, $k_8 = 0.5$, $k_9, k_{11} = 0.75$, $\zeta_1 \sim \zeta_4 = 1$.

We simulated the attitude and position control problems including altitude control. The proposed simulation results have been obtained for stabilization during the hovering around the desired position $\xi_d = [1, 1, 2] \text{ (m)}$, starting from the initial positions $\xi_0 = [0, 0, 0]$ and Euler angles $\eta = [5, -5, 10] \text{ degrees}$. The desired yaw angle has been chosen to be equal to zero. The control task is to stabilize the attitude of quadrotor while following the desired position ξ_d . For comparisons, we simulated other nonlinear controllers [19], [23] with same control tasks. As shown in Fig. 8, we can see that the desired position is achieved by the controllers. Quantitative comparisons of simulation results are given in Table V and the proposed nonlinear controller

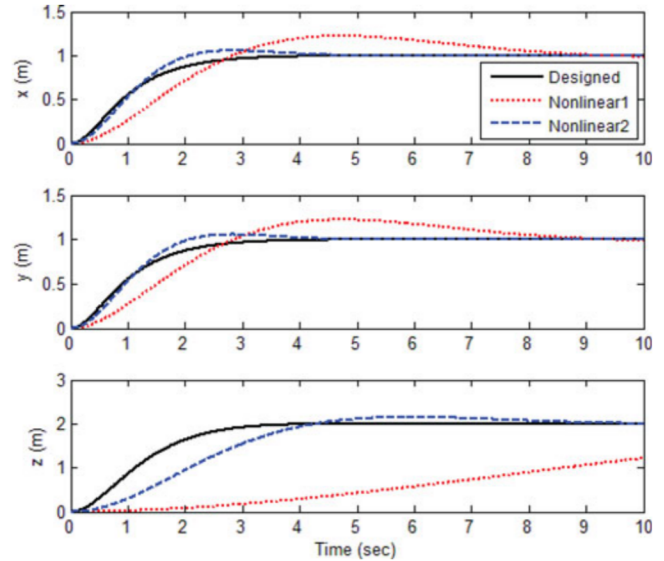


Fig. 8. Simulation results of position control.

TABLE VI
COMPARISONS OF EXPERIMENTAL RESULTS—*x*, *y* POSITIONS

Benchmarks		Range	Average	Variance	Standard deviation
Designed	<i>x</i>	2.04	0.09	0.02	0.14
	<i>y</i>	1.67	0.09	0.03	0.18
PID	<i>x</i>	2.08	0.57	0.02	0.15
	<i>y</i>	2.26	0.13	0.05	0.23
Nonlinear1 [19]	<i>x</i>	3.22	1.15	0.44	0.67
	<i>y</i>	4.58	0.20	0.81	0.90
Nonlinear2 [23]	<i>x</i>	4.79	-1.47	0.66	0.81
	<i>y</i>	3.31	0.82	0.60	0.78

shows better performance compared to other two nonlinear controllers. The roll and pitch angles are changed due to the desired roll and pitch angles which are derived by position controller. The Euler angles converge to zero as shown in Fig. 9. There is a tradeoff between the settling time and the rate of change of the Euler angles. Control inputs $U_1 \sim U_4$ are obtained by proposed controller. From the obtained control inputs, we can calculate the reference RPMs of each BLDC motor and these reference RPMs will be used to find control input PWM signal in the actual experiments.

VI. EXPERIMENTAL RESULTS

The proposed nonlinear control strategy has been tested on the ‘Arducopter’ platform as mentioned previously. Two different types of tests were carried out on the quadrotor platform to verify the designed controller. One of the tests is the autonomous takeoff and hovering flight test while keeping the initial position. Another is the point tracking test while maintaining the desired altitude. Experimental tests are performed outside to obtain the GPS sensor data as shown in Fig. 10, and all physical and control

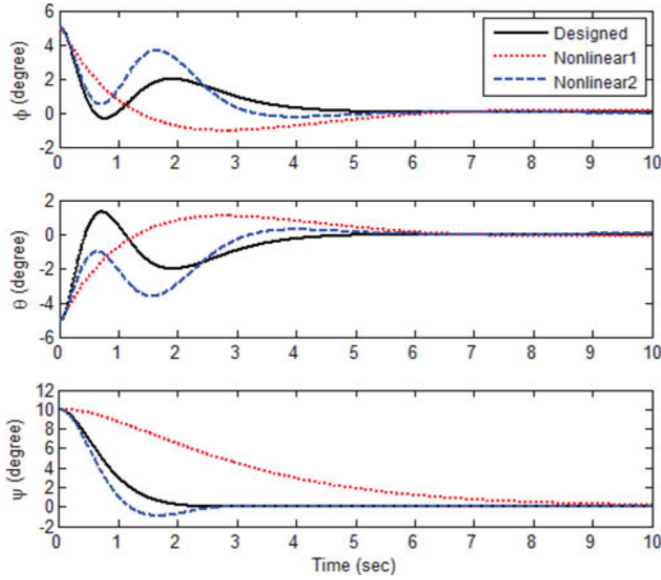


Fig. 9. Simulation results of Euler angles.

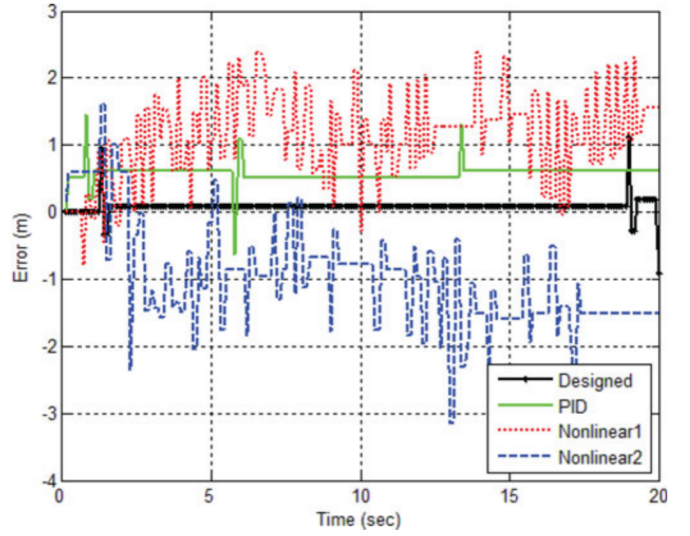
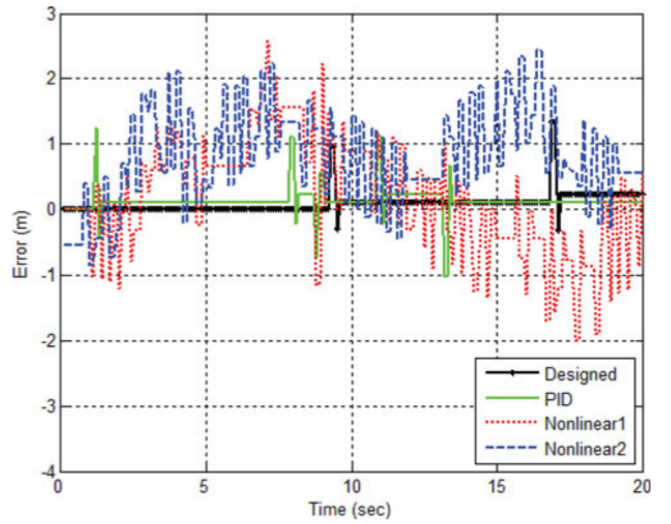


Fig. 10. Autonomous hovering test in flight.

parameters are the same as simulation results. We used filtered GPS data which are manipulated by Arducopter manufacturer. The temperature is approximately 12 °C and wind speed was estimated around 1 ~ 2 m/s.

In the first experiment, the objective is to make the quadrotor hover at an altitude of 1.5 (m) after autonomous take-off and the position of quadrotor is fixed at the starting point. We have compared our method with other control methods such as PID controller and nonlinear controllers proposed in [19], [23]. Figs. 11 and 12 and Table VI show the x , y position errors of the hovering test, and Fig. 13 illustrates the altitude error of the hovering test. As shown in these figures, the designed nonlinear controller shows better performance among four different controllers. In detail, we can observe that the PID controller has steady state errors and overshoot in the Fig. 13 while it has a fast settling time. The other nonlinear control 1 [19] scheme has

¹The PID gains used in the tests are the gains tuned by Arducopter manufacturer.

Fig. 11. Experimental result of position error x (Take-off).Fig. 12. Experimental result of position error y (Take-off).

slow settling time compared with other three methods, and it has some oscillations. When considering the position accuracy of GPS sensor, which is less than 3 m given by manufacturer, position errors of designed controller are acceptable range during flights in outdoor. There are some peak points of x , y errors in Figs. 11 and 12 which are caused by GPS errors. The performance of altitude controller is good enough to validate the designed controller where the altitude error is less than 0.1 (m). Figs. 14 and 15 depict the roll and pitch Euler angles of each method. The designed nonlinear controller has small deviation compared with other three methods. The PID controller also has small deviation; however, there are some overshoots in the graph as shown in Fig. 14. Note that the yaw angle was not being controlled; therefore it is not shown in the results. There exists some oscillations which are caused by the position controller

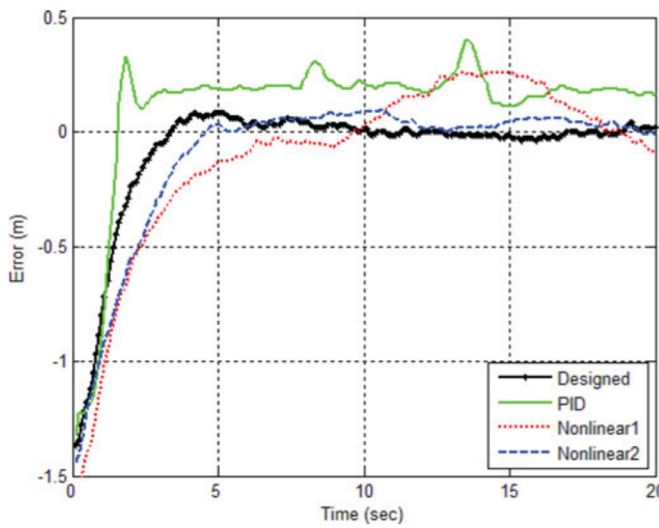


Fig. 13. Experimental result of the altitude error (Take-off).

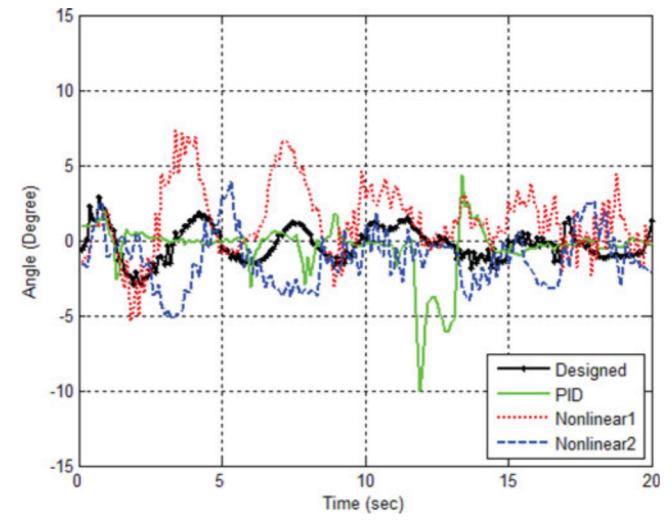


Fig. 15. Experimental result of the pitch angle (Take-off).

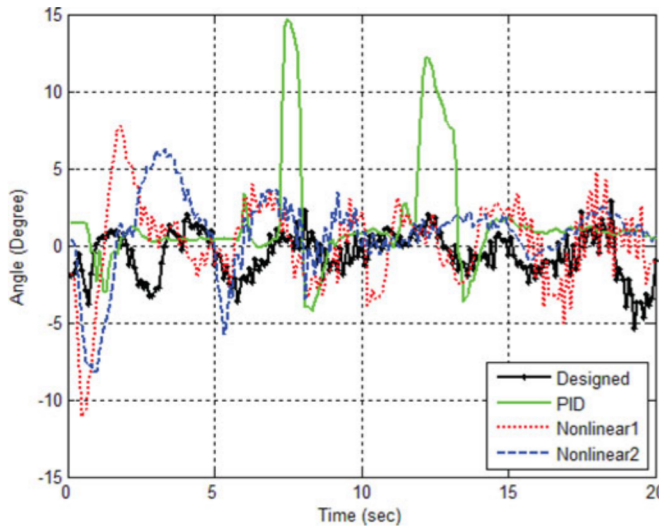


Fig. 14. Experimental result of the roll angle (Take-off).

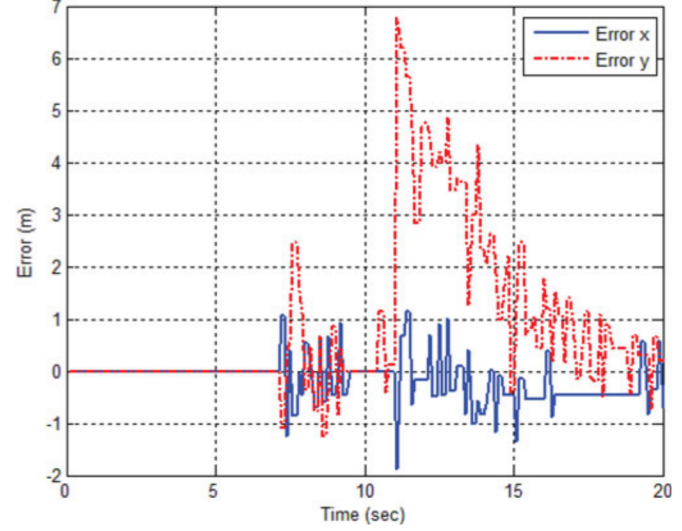


Fig. 16. Experimental result of position errors (Tracking).

to maintain the desired position and disturbances; however, the attitude of quadrotor is keeping the stability without loss of control. When considering disturbances in outdoor experiments such as wind and atmosphere, the performance of designed nonlinear controller is acceptable. Experimental results show that the designed nonlinear controller has the better performance compared with other control methods.

Autonomous point tracking task is assigned in the second experiment. The desired position will be changed about 10 s after take-off, and the quadrotor will be moved to the y direction approximately 7 m away from the initial position. Fig. 16 presents x , y position errors and Fig. 17 shows the altitude error of quadrotor. After take-off, there are some oscillations in y -direction caused by GPS errors or disturbances from environment. The desired position will be changed after 10 s later,

and we can verify that the error y was decreased by the designed controller. When changing the desired position, we can observe small overshoot in altitude error; however, the altitude error is less than 0.1 m. The quadrotor reaches at the desired position while keeping the desired altitude within the margins of hardware error. As can be seen above simulations and experiments, good performance is achieved by the proposed controller for autonomous take-off, hovering, and tracking experiments in outdoor.

From our experiments, we have obtained quite good results; however, our experiments have some limitations arising from outdoor environments such as wind speed, temperature, and weather (atmospheric pressure). We have tried to test all experiments under the same conditions, but there would be some small changes in these conditions. These small variations could have

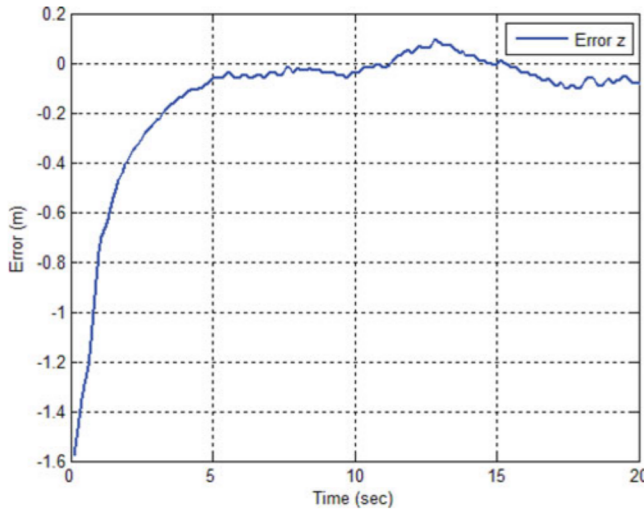


Fig. 17. Experimental result of the altitude error (Tracking).

influences on sensors in quadrotor system and results. These problems are associated with robustness or adaptive control problems of quadrotor system. We will mention these problems in future works.

VII. CONCLUSION AND FUTURE WORK

In this paper, a new nonlinear controller has been proposed to track the position and to stabilize the attitude of quadrotor. The designed controller is implemented into the quadrotor system. Quadrotor dynamics are derived by using the *Euler–Lagrangian* approach and all physical parameters in dynamics, which are obtained experimentally based on the related theory, are considered in applying the nonlinear control algorithm into the quadrotor. Details of hardware components are introduced and the stability analysis has been addressed by using the Lyapunov stability theorem. The proposed control scheme has been successfully applied to the fully autonomous quadrotor system. Simulation and experimental results are shown that the designed controller performs satisfactorily. As far as the authors are concerned, this paper is the first one that successfully implements nonlinear control algorithms into an underactuated quadrotor including all physical parameter problems and outdoor experiments.

Our future works will be extended into several directions to increase the accuracy. First, the speed of motor will be measured by using additional sensor for a feedback control. We measured the relation between the input PWM and output RPM in this paper; however, this relation depends on the capacity of battery. By sensing the motor speed, we can control the quadrotor system more precisely. Second, the sensor fusion method will be used to increase precision in position and attitude data. Finally, the robust or adaptive control method will be considered to cope with changes in environment or parametric uncertainties such as the moment of inertia and aerodynamics effects.

REFERENCES

- [1] A. Tayebi and S. McGilvray, "Attitude stabilization of a vtol quadrotor aircraft," *IEEE Trans. Control Syst. Technol.*, vol. 14, no. 3, pp. 562–571 May 2006.
- [2] B. Erginer and E. Altug, "Modeling and pd control of a quadrotor vtol vehicle," in *Proc. IEEE Intell. Vehicles Symp.*, 2007, pp. 894–899.
- [3] S. Bouabdallah and R. Siegwart, "Full control of a quadrotor," in *Proc. IEEE/RSJ Int. Intell. Robots Syst. Conf.*, 2007, pp. 153–158.
- [4] S. Bouabdallah, P. Murrieri, and R. Siegwart, "Design and control of an indoor micro quadrotor," in *Proc. IEEE Int. Conf. Robot. Autom. Conf.*, 2004, vol. 5, pp. 4393–4398.
- [5] G. Hoffmann, H. Huang, S. Waslander, and C. Tomlin, "Quadrotor helicopter flight dynamics and control: Theory and experiment," in *Proc. AIAA Guidance, Navigation, Control Conf.*, 2007, pp. 1–20.
- [6] J. Li, and Y. Li, "Dynamic analysis and pid control for a quadrotor," in *Proc. IEEE Int. Conf. Mechatronics Autom. Conf.*, 2011, pp. 573–578.
- [7] A. L. Salih, M. Moghavemi, H. A. Mohamed, and K. S. Gaeid, "Modelling and pid controller design for a quadrotor unmanned air vehicle," in *Proc. IEEE Int. Conf. Autom. Quality Testing Robot. Conf.*, 2010, vol. 1, pp. 1–5.
- [8] S. Bouabdallah, A. Noth, and R. Siegwart, "Pid versus lq control techniques applied to an indoor micro quadrotor," in *Proc. IEEE/RSJ Int. Conf. Intell. Robots Syst.*, 2004, vol. 3, pp. 2451–2456.
- [9] H. Voos, "Nonlinear control of a quadrotor micro-uav using feedback-linearization," in *Proc. IEEE Int. Conf. Mechatronics.*, 2009, pp. 1–6.
- [10] D. Lee, H. J. Kim, and S. Sastry, "Feedback linearization versus adaptive sliding mode control for a quadrotor helicopter," *Int. J. Control., Autom. Syst.*, vol. 7, no. 3, pp. 419–428, 2009.
- [11] Q.-L. Zhou, Y. Zhang, C.-A. Rabbath, and D. Theilliol, "Design of feedback linearization control and reconfigurable control allocation with application to a quadrotor uav," in *Proc. IEEE Control Fault-Tolerant Syst. Conf.*, 2010, pp. 371–376.
- [12] T. Madani and A. Benallegue, "Backstepping control for a quadrotor helicopter," in *Proc. IEEE/RSJ Int. Conf. Intell. Robots Syst.*, 2006, pp. 3255–3260.
- [13] M. Huang, B. Xian, C. Diao, K. Yang, and Y. Feng, "Adaptive tracking control of underactuated quadrotor unmanned aerial vehicles via backstepping," in *Proc. IEEE Amer. Control Conf.*, 2010, pp. 2076–2081.
- [14] T. Madani and A. Benallegue, "Sliding mode observer and backstepping control for a quadrotor unmanned aerial vehicles," in *Proc. IEEE Amer. Control Conf.*, 2007, pp. 5887–5892.
- [15] R. Xu and U. Ozguner, "Sliding mode control of a quadrotor helicopter," in *Proc. 45th IEEE Decision Control Conf.*, 2006, pp. 4957–4962.
- [16] H. Bouadi, M. Bouchouha, and M. Tadjine, "Sliding mode control based on backstepping approach for an uav type-quadrotor," *World Academy Sci., Eng. Technol.*, vol. 26, pp. 22–27, 2007.
- [17] X. Ding and Y. Yu, "Motion planning and stabilization control of a multipropeller multifunction aerial robot," *IEEE/ASME Trans. Mechatronics*, vol. 18, no. 2, pp. 645–656, Apr. 2013.
- [18] A. Das, K. Subbarao, and F. Lewis, "Dynamic inversion with zero-dynamics stabilisation for quadrotor control," *IET Control Theory Appl.*, vol. 3, no. 3, pp. 303–314, 2009.
- [19] S. Salazar-Cruz, A. Palomino, and R. Lozano, "Trajectory tracking for a four rotor mini-aircraft," in *Proc. 44th IEEE Conf. Decision Control Eur. Control Conf.*, 2005, pp. 2505–2510.
- [20] J. Escareno, S. Salazar-Cruz, and R. Lozano, "Embedded control of a four-rotor uav," in *Proc. IEEE Amer. Control Conf.*, 2006, pp. 6–pp.
- [21] P. Castillo, A. Dzul, and R. Lozano, "Real-time stabilization and tracking of a four-rotor mini rotocraft," *IEEE Trans. Control Syst. Technol.*, vol. 12, no. 4, pp. 510–516, Jul. 2004.
- [22] I. González, S. Salazar, and R. Lozano, "Chattering-free sliding mode altitude control for a quad-rotor aircraft: Real-time application," *J. Intell. Robot. Syst.*, pp. 1–19, 2013.
- [23] S. Bouabdallah and R. Siegwart, "Backstepping and sliding-mode techniques applied to an indoor micro quadrotor," in *Proc. IEEE Int. Conf. Robot. Autom.*, 2005, pp. 2247–2252.
- [24] D. L. Gabriel, J. Meyer, and F. Du Plessis, "Brushless dc motor characterisation and selection for a fixed wing uav," in *Proc. IEEE AFRICON*, 2011, pp. 1–6.
- [25] M. T. Körögülu, M. Önkol, and M. Ö. Efe, "Experimental modelling of propulsion transients of a brushless dc motor and propeller pair under

- limited power conditions: A neural network based approach," in *Proc. 2nd IFAC Int. Conf. Intell. Control Syst. Signal Process.*, 2009, pp. 21–23.
- [26] M. R. Jardin and E. R. Mueller, "Optimized measurements of uav mass moment of inertia with a bifilar pendulum," presented at the AIAA Guidance, Navigation Control Conf. Exhibit, Hilton Head, SC, USA, 2007.
- [27] R. W. Prouty, *Helicopter Performance, Stability, and Control*. Melbourne, FL, USA: Krieger 1995.
- [28] J. G. Leishman, *Principles of Helicopter Aerodynamics*. Cambridge, U.K.: Cambridge Univ. Press, 2006.
- [29] J. Wayne, *Helicopter theory*, Princeton, NJ, USA: Princeton Univ. Press, 1980.
- [30] (2012, Aug.) APC Propellers, props for model airplanes. [Online]. Available: <http://www.apcprop.com/v/index.html>



Hyo-Sung Ahn (S'04–M'06) received the B.S. and M.S. degrees in astronomy from Yonsei University, Seoul, Korea, in 1998 and 2000, respectively, the M.S. degree in electrical engineering from the University of North Dakota, Grand Forks, ND, USA, in 2003, and the Ph.D. degree in electrical engineering from Utah State University, Logan, UT, USA, in 2006.

Since July 2007, he has been with the School of Mechatronics, Gwangju Institute of Science and Technology (GIST), Gwangju, Korea. He is currently an Associate Professor and Dasan Professor. Before joining GIST, he was a Senior Researcher with the Electronics and Telecommunications Research Institute, Daejeon, Korea. He is the author of the research monograph *Iterative Learning Control: Robustness and Monotonic Convergence for Interval Systems* (Springer-Verlag, 2007). His research interests include control systems, autonomous systems, and aerospace navigation and control.



Young-Cheol Choi (S'08) received the B.S. degree in mechanical engineering from Konkuk University, Seoul, Korea, in 2007 and the M.S. degree in mechatronics from Gwangju Institute of Science and Technology (GIST), Gwangju, Korea, in 2010, where he is currently working toward the Ph.D. degree in mechatronics.

His research interests include unmanned aerial vehicles, formation control, and autonomous systems.